_ ⬝ 🟊

NASA Contractor Report 187619

ICASE Report No. 91–67

ICASE

CONTROL OF OSCILLATORY FORCES ON A CIRCULAR CYLINDER BY ROTATION

Yuh-Roung Ou

NASA

National Aeronautics and
Space Administration

Langley Research Center
Hampton, Virginia 23665-5225

CONTROL OF OSCILLATORY FORCES ON
A CIRCULAR CYLINDER BY ROTATION[1]

Yuh-Roung Ou
Institute for Computer Applications in Science and Engineering
NASA-Langley Research Center
Hampton, VA 23665

ABSTRACT

The temporal development of forces acting on a rotating cylinder is investigated numerically in response to a variety of time-dependent rotation rates. Solutions are presented for several types of rotation that illustrate significant effects of the rotation rate on lift, drag and lift/drag coefficients. Of special interest is the formulation of an optimal control problem for the case of constant speed of rotation. We find an optimal rotation rate that achieves the maximum value of time-averaged lift/drag ratio.

1. INTRODUCTION

It has been realized that the next generation of high performance aircraft must be designed to have the capability to produce high lift-to-drag ratio during certain maneuvers. Thus, it is desirable to devise an effective method to achieve such aerodynamic performance. Although various efforts have been made to improve the aerodynamic characteristics of advanced aircraft over the years, it is now commonly believed that any further gains in aerodynamics will mostly be contributed by the application of various types of flow control mechanisms [1]. Consequently, in recent years there has been increased interest in the study of control problems arising in fluid flow systems. However, the principal progress so far has been essentially accomplished by experimental investigations, while the analytical or numerical approach has been remained only in its infancy. Most recently, a successful theoretical approach has been developed by Sritharan [2, 3] for a class of optimal control problems in viscous flow. Other contributions in this area of research have been presented by Gunzburger et al. [4], Abergel and Temam [5] and Ou and Burns [6].

In the area of boundary-layer separation control, several methods have been developed experimentally to provide various effective results of flow control, for example moving surface, blowing, suction, injection of a different gas, etc. In particular, the effectiveness of the moving surfaces was demonstrated experimentally by Modi et al. [7] on an airfoil. They reported a successful experiment on boundary-layer control by placing rotating cylinders at the leading and trailing edges of an airfoil. It has been shown that this mechanism can retard the initial growth of the boundary layer, with important consequences for lift enhancement and stall delay. In spite of the fact that considerable aerodynamic benefits were gained by changing the cylinder speed ratio, in their experiments the speed of rotation was restricted to constant values. However, in an unsteady flow, a constant rotation rate of a rotating cylinder may not correspond to the optimal performance when an airfoil is undergoing a rapid maneuver. This motivated us to consider the fundamental problem regarding the unsteady flow control. We therefore propose a model for the numerical study of controlling the temporal development

1

of the flow field around a circular cylinder. As adopted by Modi's work, a moving boundary control mechanism is employed, i.e. rotation of the cylinder.

The main thrust of the current investigation is on simulation and control of an unsteady flow generated by a circular cylinder undergoing a combined (steady or unsteady) rotatory and rectilinear motion. In the past few decades, although many investigations associated with rotating cylinders have been made experimentally [8, 9, 10] and numerically [11, 12, 13, 14], most of these works are primarily concerned with the effect of rotation rate upon the vortex shedding process. It appears that the effect of the rotation rate on the forces exerted by the fluid has received far less attention despite the fact that it has important practical engineering applications.

In this paper we report the numerical results of the temporal development of forces on the rotating cylinder response to a variety of time-dependent rotation rates. Precise understanding of this moving surface mechanism in boundary layer control may provide an effective way for lift enhancement and drag reduction. By treating the rotation rate as a control variable in this model, we will eventually be interested in finding the optimal control (i.e. the optimal trajectory of the rotation rate) that maximizes the lift-to-drag ratio over a fixed time interval. We hope this study will serve as a guide on the formulation of optimal flow control problems, lead to possible implementation of a computational algorithm to calculate the optimal solution, and ultimately contribute a useful systematic algorithm for many practical control designs of high-performance aircraft.

2. MATHEMATICAL AND NUMERICAL FORMULATIONS

We consider control problems for a two-dimensional viscous incompressible flow generated by an impulsively started circular cylinder. The cylinder is translated with a constant rectilinear speed U normal to its generator and is simultaneously rotated in the counterclockwise direction with an angular velocity $\vec{\Omega}(t)$ about its axis. This problem is investigated numerically by solving a velocity/vorticity formulation of the Navier-Stokes equations with an implementation of the Biot-Savart law. The numerical approach used in the present study is

the one developed by Chen [15] for the problem of a circular cylinder oscillating in a rectangular box. It is based on an explicit finite-difference/pseudo-spectral technique to yield time accurate solutions to the governing equations. This numerical algorithm was further modified to investigate an unsteady flow around a rotating cylinder undergoing constant rotational speeds [14], and time-dependent rotation rates [16]. Throughout the solution procedures, a particular integral representation for flow kinematics proposed by Wu and Thompson [17] provides the basic link between the velocity and vorticity fields.

2.1 Governing Equations

For a two-dimensional unsteady viscous flow in incompressible fluid, the dimensionless Cartesian coordinate form of the governing equations for vorticity and velocity can be written as

$$\frac{\partial \omega}{\partial t} + \vec{u} \cdot \nabla \omega = \frac{2}{Re} \nabla^2 \omega \tag{1}$$

and

$$\nabla^2 \vec{u} = -\nabla \times (\omega \vec{e}_z). \tag{2}$$

The cylinder radius a is used as the length scale while a/U is used as the time scale. The Reynolds number $Re = 2Ua/\nu$ is based on the cylinder diameter $2a$ and the magnitude U of the rectilinear velocity.

A nonrotating reference frame translating with the cylinder is employed. In this frame the dimensionless boundary conditions for the problem of a rotating cylinder can be written as

$$\begin{cases} \vec{u} = -\alpha(t)y\vec{e}_x + \alpha(t)x\vec{e}_y & \text{for } (x, y) \in \Gamma \\ \vec{u} = \vec{e}_x & \text{for } \sqrt{x^2 + y^2} \to \infty, \end{cases} \tag{3}$$

where Γ denotes the impermeable solid boundary of the cylinder B. The angular/rectilinear speed ratio $\alpha(t) = \Omega(t)a/U$ is the primary control parameter in this paper.

This velocity/vorticity formulation is especially well suited to treating initial development of the flow generated by impulsively started bodies in which a relatively small vortical viscous

region is embedded in a much larger inviscid potential flow. Consequently, the computational domain may be restricted to a smaller region where the vorticity contributions are contained.

2.2 Integral Representation For Flow Kinematics

In the simulation of an exterior flow problem, one of the difficulties encountered is that of prescribing the appropriate nonvelocity boundary conditions at the solid surface. In particular, the numerical method based on the velocity/vorticity formulation will require the boundary vorticity values at the solid surface in the solution procedure. This difficulty can be overcome by the application of an integral representation for the kinematics of flow field. This kinematic relationship between velocity and vorticity fields on the domain is known as the generalized Biot-Savart law of induced velocity

$$
\vec{u}(\vec{r_0}, t) = -\frac{1}{2\pi} \int \int_D \frac{\vec{\omega}(\vec{r}, t) \times (\vec{r} - \vec{r_0})}{|\vec{r} - \vec{r_0}|^2} dA
$$
$$
-\frac{1}{2\pi} \int \int_B \frac{2\vec{\Omega}(\vec{r}, t) \times (\vec{r} - \vec{r_0})}{|\vec{r} - \vec{r_0}|^2} dA + \vec{U}, \tag{4}
$$

where D is the region occupied by the fluid. Here $\vec{r_0}$ represents the field point located in the domain where the velocity is evaluated. Thus, the boundary vorticity values can be obtained by setting the surface nodes as the field point $\vec{r_0}$ in (4).

In fact, this integral representation not only allows one to obtain boundary vorticity on the solid surface but also can determine the velocity point-by-point explicitly if all vorticity values are known everywhere in the domain of interest. Moreover, it often exhibits more realistic behavior at the outer perimeter of the computational domain than asymptotic techniques used in other formulations. This indicates that the difficulty resulting from the imposed far-field condition is removed by the application of this integral constraint, provided that no vorticity escapes from the computational domain.

2.3 Numerical Solution Procedure

In order to accommodate problems of a time-dependent domain, Eqs. (1) and (2) can be recast into a body-fitted coordinate system. This coordinate allows one to deal with

4

an unsteady flow problem for computing any arbitrary body shapes (or even with moving boundaries) on a fixed computational rectangular grid, and the interpolation of the grid points and boundary conditions in the physical space are not necessary.

The vorticity transport Eq. (1) and Poisson Eq. (2) can be written in term of time-varying generalized body-fitted coordinate system (ξ, η) as follows:

$$
\begin{aligned}
\omega_t = & \frac{x_t}{J}(\omega_\xi y_\eta - \omega_\eta y_\xi) - \frac{y_t}{J}(\omega_\xi x_\eta - \omega_\eta x_\xi) \\
& - \frac{1}{J}[y_\eta(u\omega)_\xi - y_\xi(u\omega)_\eta + x_\eta(v\omega)_\xi - x_\xi(v\omega)_\eta] \\
& + \frac{2}{ReJ^2}(\sigma\omega_{\xi\xi} - 2\beta\omega_{\xi\eta} + \gamma\omega_{\eta\eta}) + \frac{2}{Re}(P\omega_\xi + Q\omega_\eta),
\end{aligned} \tag{5}
$$

and

$$
\begin{cases}
\sigma u_{\xi\xi} - 2\beta u_{\xi\eta} + \gamma u_{\eta\eta} + J^2(Pu_\xi + Qu_\eta) = J(x_\eta\omega_\xi - x_\xi\omega_\eta), \\
\sigma v_{\xi\xi} - 2\beta v_{\xi\eta} + \gamma v_{\eta\eta} + J^2(Pv_\xi + Qv_\eta) = J(y_\eta\omega_\xi - y_\xi\omega_\eta),
\end{cases} \tag{6}
$$

where

$$
\begin{cases}
\sigma = x_\eta^2 + y_\eta^2, & \beta = x_\xi x_\eta + y_\xi y_\eta, & \gamma = x_\xi^2 + y_\xi^2, \\
P = \xi_{xx} + \xi_{yy}, & Q = \eta_{xx} + \eta_{yy}, & J = x_\xi y_\eta - x_\eta y_\xi.
\end{cases} \tag{7}
$$

The vorticity transport Eq. (5) is first discretized by a second order central difference in the radial direction and a pseudospectral transform method in the circumferential direction for all spatial derivatives. This semi-discretization form of Eq. (5), consisting of a system of ordinary differential equations in time can be written as

$$
\frac{d\hat{\omega}}{dt} = F(\hat{\omega}), \quad \hat{\omega} = (\omega_{2,2}, \cdots, \omega_{M-1,N-1})^T, \tag{8}
$$

for all the interior grid points. Therefore, the calculation procedure to advance the solution for any given time increment can be summarized as follows:

Step 1: Internal vorticity over the fluid region at each interior field point is calculated by solving the discretized vorticity transport equation. An explicit second-order rational Runge-Kutta marching scheme based on the work of [18] is used to advance in time for (8):

$$
\hat{\omega}^{n+1} = \hat{\omega}^n + \frac{2\hat{g}_1(\hat{g}_1, \hat{g}_3) - \hat{g}_3(\hat{g}_1, \hat{g}_1)}{(\hat{g}_3, \hat{g}_3)}, \tag{9}
$$

$$
\begin{cases}
\hat{g}_1 = F(\hat{\omega}^n)\Delta t \\
\hat{g}_2 = F(\hat{\omega}^n + 0.5\hat{g}_1)\Delta t \\
\hat{g}_3 = 2\hat{g}_1 - \hat{g}_2
\end{cases} \tag{10}
$$

5

where $(\hat{\cdot}, \hat{\cdot})$ denotes the scalar product.

Step 2: Using known internal vorticity values at all the interior grid points from step 1, Eq. (4) is used to update the boundary vorticity values at all the surface nodes. In Eq. (4), $\vec{r_0}$ represents all grid points located on the solid boundary.

Step 3: At this stage, all the vorticity values in the computational domain are known at the new time level. Then, the velocity at points on the outer perimeter of the computational domain are calculated by the integral kinematic constraint. In Eq. (4), $\vec{r_0}$ now denotes the points located on the outer perimeter of the computational domain.

Step 4: The new velocity field can be established by solving the Poisson Eq. (6) with prescribed solid boundary conditions and outer boundary conditions that have been determined from step 3. The resulting discretized Poisson equation is an 11-banded matrix equation. It is then solved by a preconditioned biconjugate gradient routine [19]. This step completes the computational loop for each time level.

One further important point to be noted in this integral approach is the determination of the initial flow field. This integral approach enables the numerical code to generate the initial velocity field by executing one cycle of the solution procedure (from step 2 to step 4) rather than employing any additional treatments.

3. RESULTS AND DISCUSSIONS

An important consequence of the calculated solution of the velocity/vorticity formulation is that the forces can be directly evaluated from known vorticity on the cylinder surface. Hence for a known vorticity value on the cylinder surface, the lift and drag coefficients can be calculated in the r-θ coordinates as

$$C_L = \frac{2}{Re} \int_0^{2\pi} \left[-\left(\frac{\partial \omega}{\partial r} \right) + \omega \right]_\Gamma \cos \theta d\theta, \tag{11}$$

$$C_D = \frac{2}{Re} \int_0^{2\pi} \left[\left(\frac{\partial \omega}{\partial r} \right) - \omega \right]_\Gamma \sin \theta d\theta. \tag{12}$$

In particular, we denote the positive values of C_L in the $-y$ direction.

6

Although the aim of current research is to cover a wide range of all physically attainable time-dependent rotation rates, the computational experiments so far have been performed under the following three basic types of rotation: 1) time-harmonic rotatory oscillation, $\alpha(t) = A_1 \sin \pi F_1 t$; 2) time-periodic rotation, $\alpha(t) = A_2 |\sin \pi F_2 t|$; 3) constant speed of rotation, $\alpha(t) = $ constant. All variables are in the nondimensional forms. Here $F_1 = 2af_1/U, 2F_2 = 2af_2/U$ is the reduced frequency and $A_i = \pi F_i \theta_i, i = 1, 2$ is the reduced velocity of the rotation, while f_i, θ_i is denoted as the forcing frequency and the angular amplitude of the rotation, respectively.

The feasibility and accuracy of the numerical algorithm are tested by computing several particular values of constant speed of rotation at $Re = 200$. The excellent agreement is achieved for these chosen parameters against the experimental work of Coutanceau and Ménard [9]. For a more precise account of the comparison with experiments, the reader is referred to Chen et al. [14].

3.1 Time-Periodic Rotation vs. Time-Harmonic Rotatory Oscillation

In practice, when a cylinder is undergoing a time-dependent rotation with prescribed forcing frequency, then the characteristics of resulting flow field and force responses will be essentially affected by two competing frequencies, i.e. the natural frequency and the forcing frequency. It has been shown that at $Re = 200$, the natural frequency for a nonrotating circular cylinder ($\alpha = 0$) is about $F_n = 0.18$. We first show numerical results of a forcing frequency which lies in the neighborhood of the natural frequency. The temporal evolutions of lift/drag are drawn separately in Fig. 1(a) for a time-periodic rotation $\alpha(t) = |\sin 0.25t|$ and a time-harmonic rotatory oscillation $\alpha(t) = \sin 0.5t$, respectively. In the case of time-periodic rotation, the cylinder under control is rotated in the counterclockwise direction about its axis with a time-periodic speed ratio. Notice that these two types of rotation are employed by the same forcing frequency ($F_1 = 2F_2 = 0.16$) which lies in the neighborhood of the natural frequency. The numerical results clearly confirm the expected benefit of this time-varying rotation for the lift/drag ratio. Examination of curves in Fig. 1(a) shows that

7

the system of cylinder and wake will be "locked in" by the imposed forcing frequency. This synchronization of the cylinder and wake is due to the forcing frequency of rotation which lies in the neighborhood of the natural frequency.

To demonstrate the influence of time-varying rotation, two additional values of forcing frequency were used. One is imparted to a higher forcing frequency (which is twice that of case (a)), while the other is imposed by a lower forcing frequency. Notice that neither of these frequencies are in the neighborhood of the natural frequency. The benefit of changing the rotation rate is also demonstrated in Figs. 1(b,c). In the case of time-periodic rotation, it is of interest to study the effect of forcing frequency on time-averaged lift, drag and lift/drag coefficients. Fig. 1(d) shows the variation of these time-averaged coefficients for the range of $0.08 \leq 2F_2 \leq 0.32$. The results indicate that forcing frequency has only slight effect on time-averaged coefficients.

3.2 Effect of Angular Amplitude

In the case of time-periodic rotation, there is an interest in addressing the effect of angular amplitude on the temporal evolution of forces while the forcing frequency is fixed as a constant. Fig. 2(a) shows that the lift/drag ratio on the cylinder can differ significantly at different angular amplitudes for $\alpha(t) = A|\sin 0.314t|$. Note that this plot corresponds to a reduced frequency ($2F_2 = 0.2$) which is in the neighborhood of natural frequency. Three different values of angular amplitude are considered here, $A = 1.0, 2.07$, and 3.25. Apparently, as can be seen from the figure, the larger angular amplitude yields an incremental lift/drag almost timewise over the time-span of investigation ($0 < t \leq 36$). An examination of the curve for $A = 1.0$ shows that it exhibits a clear evolution of periodicity with a frequency which is precisely equal to the input forcing frequency. Although this periodic behavior is not established for $A = 2.07$ and 3.25, their respective curves indeed exhibit an almost periodic character with respect to the time evolution.

It is also of interest to examine the effect of angular amplitude on time-average lift, drag and lift/drag coefficients. The results are shown in Fig. 2(b) for the range of $1 \leq A \leq 3.25$.

8

It illustrates that all the time-averaged force coefficients are almost linearly proportional to the angular amplitude. Significant increment in lift coefficients with increasing angular amplitude is particularly noticeable. However, slight increment in drag coefficients with increasing angular amplitude is observed.

3.3 Constant Speed of Rotation

In order to increase the magnitude of the lift and reduce the magnitude of the drag, the advantage achieved by the time-periodic rotation leads us to consider the case of constant rotation. That is, the cylinder is rotated in the counterclockwise direction about its axis with a constant speed ratio. Fig. 3(a) illustrates the temporal evolution of lift/drag coefficients by varying the speed ratio in the range of $0 < \alpha \leq 3.25$. As the speed ratio increases to 2.07, every curve exhibits a substantial timewise improvement. However, it does not imply that as the speed ratio further increases, the flow field will result in a further improvement of lift/drag ratio. On the contrary, the adverse effect of speed ratio on the lift/drag ratio is quite evident if a comparison is made between $\alpha = 3.25$ and $\alpha = 2.07$. This interesting feature leads us to consider an optimal control problem corresponding to maximize the time-averaged lift/drag coefficient for a fixed finite-time interval over the range of $0 < \alpha \leq 3.25$.

Fig. 3(b) show the effect of speed ratio on time-averaged lift, drag and lift/drag coefficients. It illustrates that the time-averaged lift is almost linearly proportional to the speed ratio, while the time-averaged drag remains as a constant value up to $\alpha = 2$, then monotonically increases with speed ratio thereafter. Most importantly, the consequence of the resulting time-averaged lift/drag demonstrates that it is *not* linearly proportional to the speed ratio. As shown in Fig. 3(b), the highest value of speed ratio $\alpha = 3.25$ is not the optimal control which corresponds to the maximum value of time-averaged lift/drag. Instead, the maximum value occurs at a lower speed ratio, approximately at $\alpha = 2.38$, and it represents a substantial increase of 440% with respect to a lower speed ratio of $\alpha = 0.5$.

4. CONCLUSIONS

A numerical method has been developed to simulate the viscous flow past a rotating cylinder with a variety of time-dependent rotation rates. The speed ratio $\alpha(t)$ can impose significant influences on the characteristics of resulting flow field as well as the temporal evolution of forces on the cylinder surface. A particular type of time-periodic rotation has been demonstrated to provide an effective way of improving lift/drag performance against the time-harmonic rotatory oscillation. Moreover, these results imply the important consequences of a proper choice of the rotation rate that corresponds to the maximum value of time-averaged lift/drag ratio.

Based on the results of this investigation, various optimal control problems may be formulated that depend on the desired performance and control restriction. In the case of constant speed of rotation, we find the optimal solution $\alpha^* = 2.38$ that maximizes the time-averaged lift/drag functional

$$J(\alpha) = \frac{1}{24} \int_0^{24} \left[\frac{C_L(t, \alpha)}{C_D(t, \alpha)} \right] dt. \tag{13}$$

The significant advantage achieved by rotation leads us to explore further the possible implementation of a computational algorithm to calculate the optimal solution for a problem without imposing any constraint on the rotation rate. Our future research will mainly focus on the algorithm to compute the optimal control laws. The tools developed here will be used to investigate the fundamental questions regarding control of separated flows by using various boundary control mechanisms.

References

[1] M. Gad-el-Hak and D. M. Bushnell, *J. Fluid Engrg.* **113**, 5 (1991).

[2] S. S. Sritharan, In *Distributed Parameter Control Systems*, 385 (Marcel Dekker, New York 1991).

[3] S. S. Sritharan, *Systems and Control Lett.* **16**, 299 (1991).

[4] M. D. Gunzburger, L. S. Hou and T. P. Svobodny, Appl. Math. Lett. **2**, 29 (1989)

[5] F. Abergel and R. Temam, *Theoret. Comput. Fluid Dynamics* **1**, 303 (1990).

[6] Y.-R. Ou and J. A. Burns, ICASE Report 91-49, (1991).

[7] V. J. Modi, F. Mokhtarian and T. Yokomizo, *J. Aircraft* **27**, 42 (1990).

[8] S. Taneda, *J. Phys. Soc. Japan* **45**, 1038 (1978).

[9] M. Coutanceau and C. Ménard, *J. Fluid Mech.* **158**, 399 (1985).

[10] P. T. Tokumaru and P. E. Dimotakis, *J. Fluid Mech.* **224**, 77 (1991).

[11] H. M. Badr and S. C. R. Dennis, *J. Fluid Mech.* **158**, 447 (1985).

[12] J. Mo, Ph.D. Thesis, U. of Tennessee Space Institute, (1989).

[13] H. M. Badr and S. C. R. Dennis, *J. Fluid Mech.* **220**, 459 (1990).

[14] Y.-M. Chen, Y.-R. Ou and A. J. Pearlstein, ICASE Report 91-10, (1991).

[15] Y.-M. Chen, Ph.D. Thesis, U. of Arizona, (1989).

[16] Y.-R. Ou, In *Meeting on Turbulence Structure and Control*, Ohio State University, April (1991).

[17] J. C. Wu and J. F. Thompson, *Computers & Fluids* **1**, 197 (1973).

[18] A. Wambecq, *Computing* **20**, 333 (1978).

[19] Y.-M. Chen, A. E. Koniges and D. V. Anderson, *Comp. Phys. Comm.* **55**, 359 (1989).
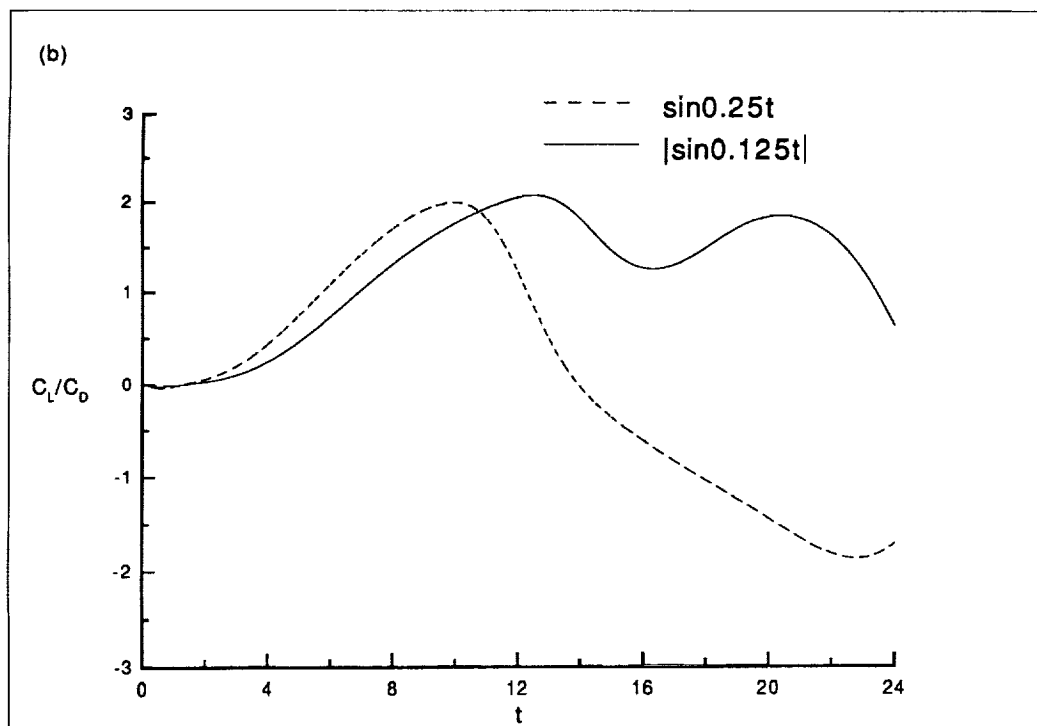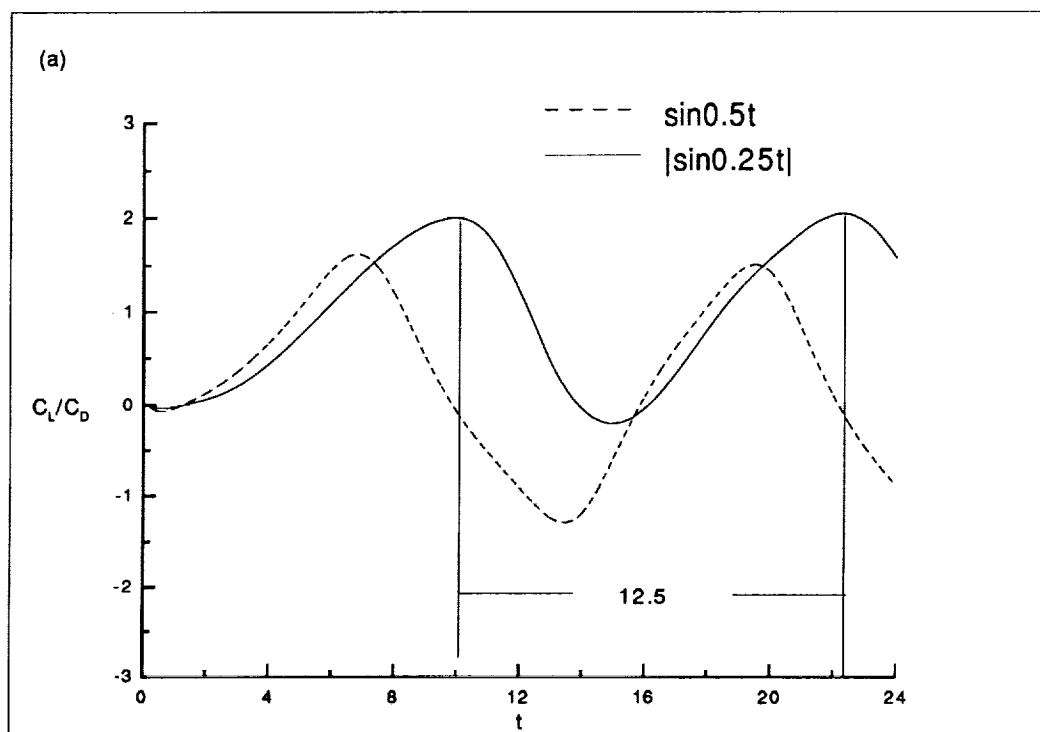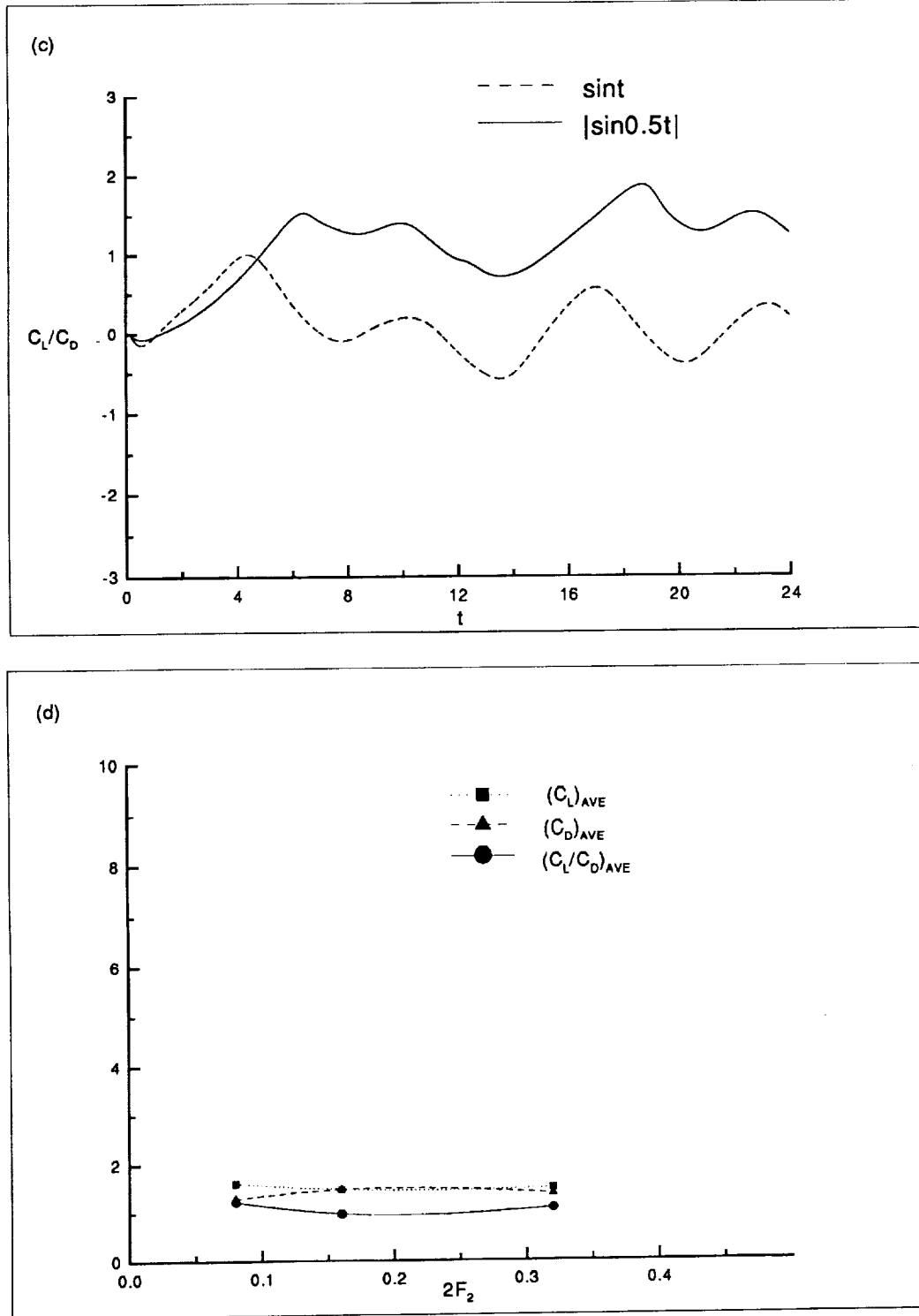
FIGURE 1 (a), (b).

FIGURE 1: Temporal evolution of lift/drag coefficients for $\alpha(t) = \sin \pi F_1 t$ and $\alpha(t) = |\sin \pi F_2 t|$. (a) $F_1 = 2F_2 = 0.16$, (b) $F_1 = 2F_2 = 0.08$, (c) $F_1 = 2F_2 = 0.32$, (d) variation of time-averaged lift, drag and lift/drag coefficients with forcing frequency.
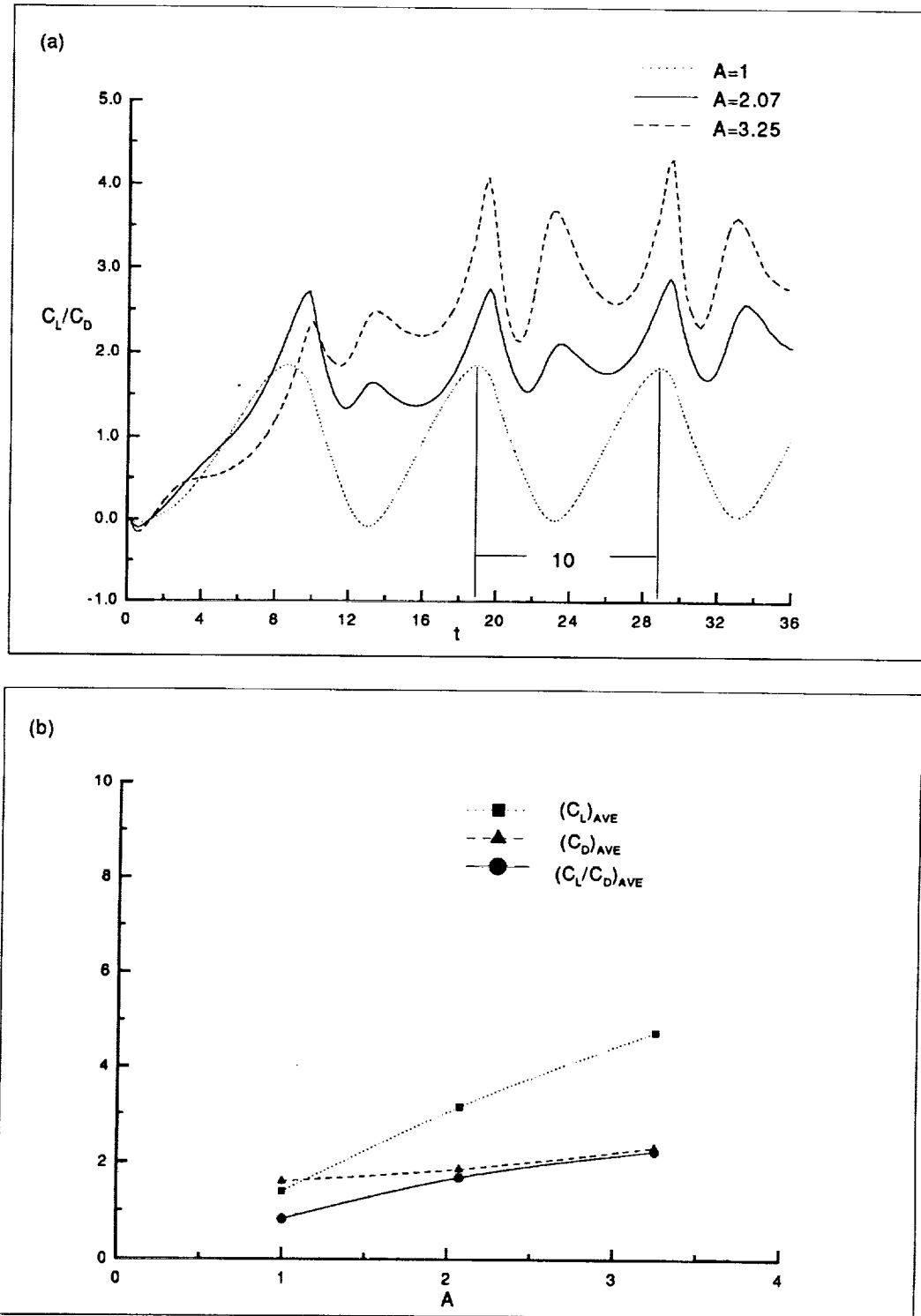
FIGURE 2: (a) Temporal evolution of lift/drag coefficients for $\alpha(t) = A|\sin 0.314t|$ at A=1.0, 2.07 and 3.25, (b) variation of time-averaged lift, drag and lift/drag coefficients with angular amplitude.
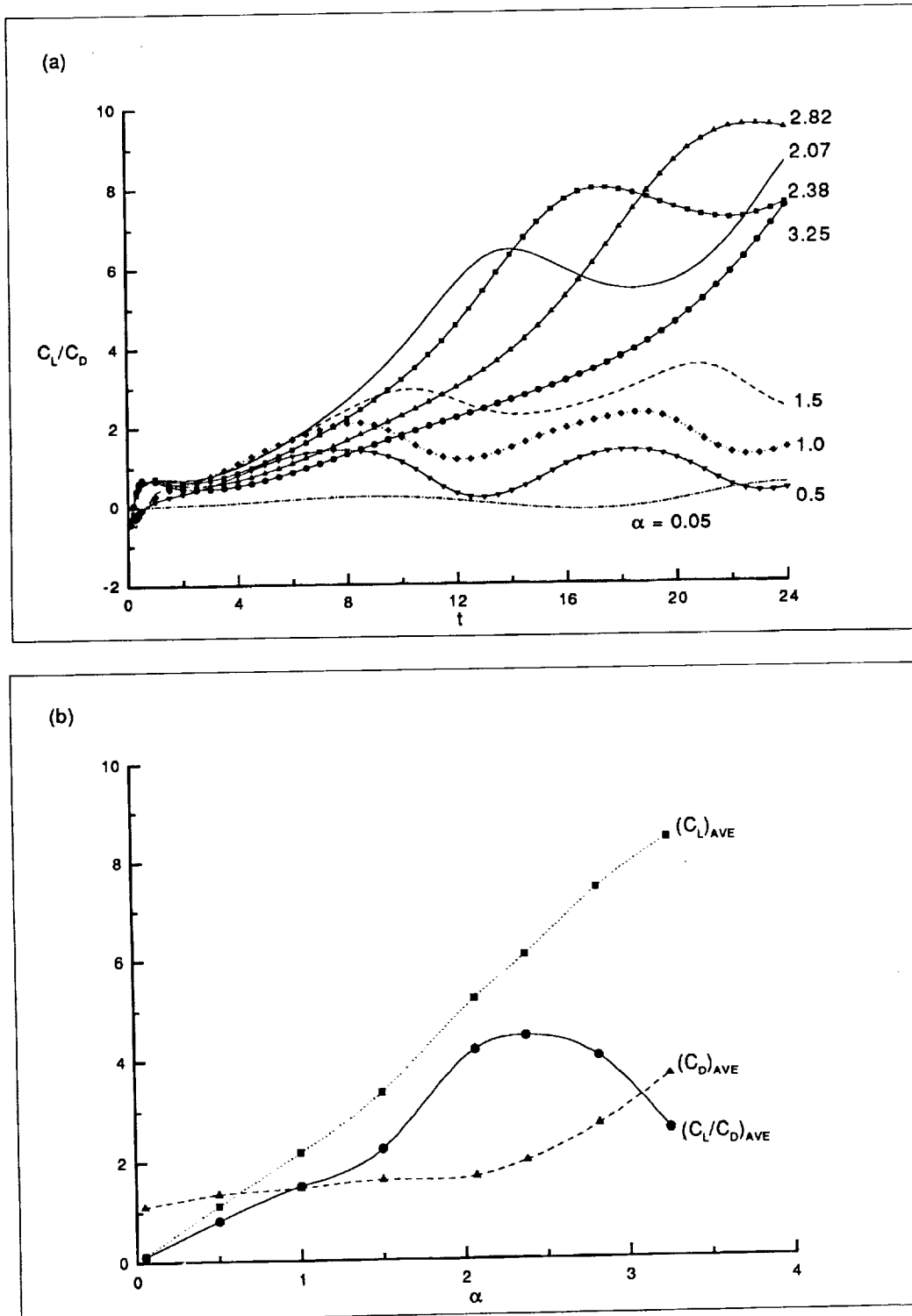
FIGURE 3: (a) Temporal evolution of the lift/drag coefficients at various values of speed ratio ($0 < \alpha \leq 3.25$), (b) effect of speed ratio on time-averaged lift, drag and lift/drag coefficients.

Report Documentation Page

1. Report No. NASA CR-187619 ICASE Report No. 91-67	2. Government Accession No.	3. Recipient's Catalog No.

4. Title and Subtitle CONTROL OF OSCILLATORY FORCES ON A CIRCULAR CYLINDER BY ROTATION	5. Report Date August 1991
	6. Performing Organization Code

7. Author(s) Yuh-Roung Ou	8. Performing Organization Report No. 91-67
	10. Work Unit No. 505-90-52-01

9. Performing Organization Name and Address Institute for Computer Applications in Science and Engineering Mail Stop 132C, NASA Langley Research Center Hampton, VA 23665-5225	11. Contract or Grant No. NAS1-18605
	13. Type of Report and Period Covered

12. Sponsoring Agency Name and Address Natiional Aeronautics and Space Administration Langley Research Center Hampton, VA 23665-5225	Contractor Report
	14. Sponsoring Agency Code

15. Supplementary Notes

Langley Technical Monitor:
Michael F. Card

To appear in...
Proc. of 4th Int'l Symposium on
Computational Fluid Dynamics,
Davis, CA, September 1991.

Final Report

16. Abstract

The temporal development of forces acting on a rotating cylinder is investigated numerically in response to a variety of time-dependent rotation rates. Solutions are presented for several types of rotation that illustrate significant effects of the rotation rate on lift, drag and lift/drag coefficients. Of special interest is the formulation of an optimal control problem for the case of constant speed of rotation. We find an optimal rotation rate that achieves the maximum value of time-averaged lift/drag ratio.

17. Key Words (Suggested by Author(s)) rotation rate, flow control	18. Distribution Statement 34 - Fluid Mechanics and Heat Transfer 63 - Cybernetics Unclassified - Unlimited

19. Security Classif. (of this report) Unclassified	20. Security Classif. (of this page) Unclassified	21. No. of pages 17	22. Price A03